

Description of the hydrogen atom and the He⁺ ion in an optical cavity using the Pauli-Fierz Hamiltonian

Yetmgeta S Aklilu¹ and Kálmán Varga^{1,*}

¹*Department of Physics and Astronomy, Vanderbilt University, Nashville, Tennessee, 37235, USA*

A system of one electron in a Coulomb potential in an optical cavity is solved using a tensor-product light-matter basis. The problem was treated at the level of the Pauli-Fierz Hamiltonian describing both light and matter quantum mechanically. The effect of cavity size on the energy levels and high harmonics generation (HHG) spectrum is studied. We have shown that the energy levels, transition states, entanglement, and the HHG spectrum can be strongly influenced by changing the cavity size.

I. INTRODUCTION

The interaction of atoms or molecules and light is usually described using a quantum description for the matter and a classical treatment for the electromagnetic fields. The potential realization of new phases of matter by engineering ultrastrong light-matter coupling led to the development of tunable ultra-small optical cavities [1, 2]. Understanding the physics of these systems requires describing the interaction of matter and light at the quantum level [3–22]. The need for quantum description has been discussed in many research works. In Refs. [9, 23] the spontaneous emission driven by a high-intensity laser pulse was investigated using perturbation theory and including the vacuum-quantized field modes. The importance of the quantum state of light in high harmonic generation was emphasized in Ref. [4]. The quantum optical aspects of HHG were also studied [7, 24–27]. The studies of the strong field ionization of atoms by quantum light [6, 28] predict new interference patterns for the tunneling electrons. The light-matter entanglement in ionization processes was also explored [29].

Model systems describing the light-matter interactions with simple analytical or numerical solutions have always played important roles in understanding complex physical systems. The interaction of light and atoms, for example, can be described by the Jaynes-Cummings model [30], which assumes a two-level atom is weakly coupled to a single mode of a quantized electromagnetic field. For strongly coupled light-matter systems [13, 31–44] no simple approach exists and the light-matter coupling cannot be treated perturbatively either.

In this work, we will study the properties of a one-electron atom or ion in a cavity using the Pauli-Fierz (PF) Hamiltonian. The PF Hamiltonian describes the interaction between quantum matters (electrons) and a massless quantized radiation field (photons) in the low-energy non-relativistic limit of quantum electrodynamics (QED) [45]. The PF approach has often been used in describing the modification of material properties in optical cavities [13, 35, 39, 41, 46].

We will use a Gaussian basis to represent the spatial variables and a Fock basis to represent the photons. The Gaussian basis is flexible enough to accurately describe the electronic states not only for the ground state but also for strong laser excitations. The Hamiltonian is diagonalized on a basis formed by the tensor product of the Gaussian states and the Fock states. We will study the dependence of the energy levels and the light-matter interaction on the cavity size. The cavity size determines the cavity frequency and the coupling strength between light and matter.

We will use time-dependent excitations to study the high-harmonic generation (HHG) and the absorption spectrum in a cavity. In this case the time-dependent Schrödinger equation will be solved by time propagation and the absorption and HHG spectrum will be calculated using the time-dependent dipole moment. HHG is a coherent source of extreme ultraviolet emission and many advances in attoscience are based on HHG. We will show the light-matter coupling leads to many additional peaks in the HHG spectrum.

II. FORMALISM

We will consider a rectangular cavity with perfectly conducting walls and use the Coulomb gauge $\nabla \cdot \mathbf{A} = 0$. The sides of the rectangular cavity are L_x , L_y , and L_z . The cavity modes are defined by the momentum vectors $k_x = \frac{n_x \pi}{L_x}$, $k_y = \frac{n_y \pi}{L_y}$, $k_z = \frac{n_z \pi}{L_z}$, where n_x, n_y, n_z are $0, 1, 2, \dots$. The cavity frequency is $\omega_{\mathbf{k}} = c|\mathbf{k}|$ and the mode functions are

$$\mathbf{S}_{\mathbf{k}\nu}(\mathbf{r}) = \sqrt{\frac{23}{V}} \begin{pmatrix} \epsilon_{\mathbf{k}\nu}^{(x)} \cos(k_x x) \sin(k_y y) \sin(k_z z) \\ \epsilon_{\mathbf{k}\nu}^{(y)} \sin(k_x x) \cos(k_y y) \sin(k_z z) \\ \epsilon_{\mathbf{k}\nu}^{(z)} \sin(k_x x) \sin(k_y y) \cos(k_z z) \end{pmatrix} \quad (1)$$

where $V = L_x L_y L_z$, ν is the polarization index, and $\epsilon_{\mathbf{k}\nu}$ is the polarization vector. These mode functions satisfy the perfect conductor boundary conditions $\mathbf{n} \times \mathbf{E}_{\perp} = 0$, $\mathbf{n} \times \mathbf{A} = 0$.

Using this mode functions the quantized vector poten-

* kalman.varga@vanderbilt.edu

tial operator and electromagnetic fields are defined as

$$\begin{aligned}\hat{\mathbf{A}}(\mathbf{r}, t) &= \sum_{\mathbf{k}\nu} \sqrt{\frac{c^2}{\epsilon_0}} \hat{q}_{\mathbf{k}\nu}(t) \mathbf{S}_{\mathbf{k}\nu}(\mathbf{r}) \\ \hat{\mathbf{E}}_{\perp}(\mathbf{r}, t) &= -\frac{1}{c} \partial_t \hat{\mathbf{A}}(\mathbf{r}, t) \\ \hat{\mathbf{B}}(\mathbf{r}, t) &= \frac{1}{c} \nabla \times \hat{\mathbf{A}}(\mathbf{r}, t),\end{aligned}\quad (2)$$

where $\hat{q}_k \doteq \hat{q}_{\mathbf{k}\nu}$ is connected to the the creation and annihilation operators

$$\begin{aligned}\hat{q}_k &= \left(\frac{\hbar}{2\omega_k}\right)^{1/2} (\hat{a}_k^\dagger + \hat{a}_k) \\ \hat{p}_k &= i \left(\frac{\hbar\omega_k}{2}\right)^{1/2} (\hat{a}_k^\dagger - \hat{a}_k)\end{aligned}\quad (3)$$

and \hat{a}_i satisfies $[\hat{a}_i, \hat{a}_j^\dagger] = \delta_{ij}$.

The Hamiltonian is defined as

$$\begin{aligned}\hat{H} &= \frac{1}{2m} \left(\hat{p} - \frac{e}{c} \hat{\mathbf{A}}\right)^2 - \frac{Z}{r} + V_{ext}(\mathbf{r}, t) + \hat{H}_{ph} \\ \hat{H}_{ph} &= \frac{\epsilon_0}{2} \int d\mathbf{r} \hat{\mathbf{E}}_{\perp}(\mathbf{r})^2 + c^2 \hat{\mathbf{B}}(\mathbf{r})^2 \\ &= \frac{1}{2} \sum_k \hat{p}_k^2 + \omega_k^2 \hat{q}_k^2,\end{aligned}\quad (4)$$

where V_{ext} is a time-dependent external field, e.g. a classical laser field.

One can use a unitary transformation to transform the Hamiltonian into length gauge [35, 47]

$$\hat{H}_L = U^\dagger \hat{H} U, \quad (5)$$

with

$$U = \exp\left\{-\frac{i}{\hbar} \hat{\mathbf{A}} \cdot \mathbf{D}\right\}, \quad (6)$$

where $\mathbf{D} = -e\mathbf{r}$ is the dipole moment.

After a straightforward calculation [35] one has

$$\hat{H}_L = \hat{H}_m + \sum_k \frac{1}{2} \left[\hat{p}_k^2 + \omega_k^2 \left(\hat{q}_k - \frac{\boldsymbol{\lambda}_k \cdot \mathbf{D}}{\omega_k} \right)^2 \right], \quad (7)$$

where

$$\hat{H}_m = -\frac{\hbar^2}{2m} \nabla^2 - \frac{Z}{r} + V_{ext}(\mathbf{r}, t) \quad (8)$$

and

$$\boldsymbol{\lambda}_k = \frac{\mathbf{S}_{\mathbf{k}\nu}(\mathbf{r})}{\sqrt{\epsilon_0}}. \quad (9)$$

We will use atomic units in the rest of the paper, $\hbar = m = e = 1$, $\epsilon_0 = \frac{1}{4\pi}$ and $c = \frac{1}{\alpha}$ (where $\alpha \approx \frac{1}{137}$ is the fine structure constant).

The trial wave function is written as

$$\Phi_i(\mathbf{r}) = \sum_{j, \mathbf{n}} a_{i,j}^{\mathbf{n}} \phi_j^{\mathbf{n}}(\mathbf{r}) \quad (10)$$

where

$$\phi_j^{\mathbf{n}}(\mathbf{r}) = \phi_j(\mathbf{r}) |\mathbf{n}\rangle \quad (11)$$

and the Fock state basis

$$|\mathbf{n}\rangle = |n_1\rangle_{\omega_1} |n_2\rangle_{\omega_2} \dots |n_M\rangle_{\omega_M}. \quad (12)$$

For the calculations we need H the matrix elements of the Hamilton operator

$$\langle \phi_i^{\mathbf{n}} | H_L | \phi_j^{\mathbf{m}} \rangle = h_{ij} \delta_{\mathbf{nm}} + c_{ij}^{\mathbf{nm}}. \quad (13)$$

The first term is a Hamiltonian where the different Fock states are not coupled

$$h_{ij} = \langle \phi_i | \hat{H}_m + \sum_{k=1}^M \left[\omega_k \left(n_k + \frac{1}{2} \right) + \frac{1}{2} (\boldsymbol{\lambda}_k \cdot \mathbf{D})^2 \right] | \phi_j \rangle \quad (14)$$

and the coupling part

$$\begin{aligned}c_{ij}^{\mathbf{nm}} &= \langle \phi_i | \mathbf{D} | \phi_j \rangle \sum_{k=1}^M \boldsymbol{\lambda}_k \omega_k \langle \mathbf{n} | \hat{q}_k | \mathbf{m} \rangle \\ &= \langle \phi_i | \mathbf{D} | \phi_j \rangle \sum_{k=1}^M \boldsymbol{\lambda}_k \sqrt{\frac{\omega_k}{2}} q_{n_k m_k} \prod_{j=1, j \neq k}^M \delta_{n_j, m_j}\end{aligned}\quad (15)$$

with

$$q_{nm} = \sqrt{n} \delta_{nm-1} + \sqrt{n+1} \delta_{nm+1}. \quad (16)$$

Finally, the overlap matrix, O of the basis functions are given by

$$\langle \phi_i^{\mathbf{n}} | \phi_j^{\mathbf{m}} \rangle = \langle \phi_i | \phi_j \rangle \delta_{\mathbf{nm}}. \quad (17)$$

If the coupling in Eq. (16) is weak and the self-dipole interaction (the last term in Eq. (14)) is small, then the approximate eigenvalues will be the sum of the eigenenergy of the Hydrogen atom E_i and the energy of the harmonic oscillators, $E_i + \sum_{k=1}^M \omega_k (n_k + 1/2)$ for each i . As we will show later, ω_k strongly increases when one decreases the volume of the cavity. This shifts the energy levels upwards. But when the cavity volume becomes smaller the coupling and the dipole self-interaction become stronger and this approximation is not valid anymore.

Gaussian basis functions are used to represent the spatial wave function:

$$\phi_i(\mathbf{r}) = N_i x^{l_i} y^{m_i} z^{n_i} \exp(-\alpha_i \mathbf{r}^2), \quad (18)$$

where

$$N_i = \left(\frac{2\alpha}{\pi}\right)^{3/4} \left[\frac{(8\alpha)^{l+m+n} l! m! n!}{(2l)! (2m)! (2n)!} \right]^{1/2}. \quad (19)$$

One could use hydrogenic eigenfunctions for the expansion but the Gaussians have better flexibility in describing the long density tails caused by the laser field. The matrix elements of the Gaussian basis functions are readily available [48–51].

For ground-state calculations the generalized eigenvalue problem of the Hamiltonian and overlap matrix is solved. For time-dependent calculations the time-dependent Schrödinger equation

$$\frac{\partial}{\partial t}\Psi = H_L\Psi \quad (20)$$

is solved by time propagation using the Crank-Nicolson method. Ψ is defined using the same basis states but with time-dependent linear combination coefficients

$$\Psi(t) = \sum_{j,\mathbf{n}} a_j^{\mathbf{n}}(t)\phi_j^{\mathbf{n}}(\mathbf{r}). \quad (21)$$

The Crank-Nicolson time propagation is defined as

$$C(t + \Delta t) = \frac{O - \frac{1}{2}H\Delta t}{O - \frac{1}{2}H\Delta t}C(t), \quad (22)$$

where $C(t)$ is the vector of the coefficients in Eq. (21) and the starting wave function $\Psi(t = 0)$ is the ground state wave function.

The high harmonic spectrum is calculated using the dipole acceleration:

$$I(\omega) = \left| \int_0^T \frac{\partial^2 d(t)}{\partial t^2} e^{-i\omega t} dt \right|^2, \quad (23)$$

$$d(t) = \langle \Psi(t) | D_z | \Psi(t) \rangle. \quad (24)$$

One can also define the component of the dipole moment in a given photon space by

$$d_{\mathbf{n}}(t) = \sum_j (a_j^{\mathbf{n}}(t))^2 \langle \phi_j^{\mathbf{n}} | D_z | \phi_j^{\mathbf{n}} \rangle, \quad (25)$$

and the total dipole will be the sum of these contributions due to the orthogonality of the Fock space basis functions. To calculate the high harmonic spectrum, we time propagate a system subjected to a classical laser pulse

$$V_{ext}(t) = E_0 e^{\frac{(t-t_0)^2}{\tau^2}} \sin(\omega_h t) D_z \quad (26)$$

and calculate $d(t)$, and then extract $I(\omega)$.

The time-dependent dipole moment will also be used to calculate the optical absorption cross-section using

$$S(E) = \frac{1}{q} \int (d(t) - d(0)) e^{iEt} d(t), \quad (27)$$

where q is the strength of the exciting potential

$$V_{ext}(t) = q\delta(t)z. \quad (28)$$

III. RESULTS AND DISCUSSION

We place the atom into the center of the cavity, at $(L_x/2, L_y/2, L_z/2)$, choose $\epsilon_k = (1, 0, 0)$ for the polarization vector and use $\lambda_k = \lambda\epsilon_k$. To keep ω_k close to the excitation energies of the system one needs large L_x, L_y and L_z , but this leads to weaker coupling (see Eq. (1)). We will test rectangular cavities with sides from a few nanometers to a few hundred nanometers. A recent review of subnanometer gap picocavities can be found in Ref. [2].

The H atom and the He⁺ ion will be used in the simulation. Eq. (16) shows that nonzero dipole matrix elements couple the light and the matter states. The simplest example of these is the dipole matrix element between the 1s ground and 2p excited state (there are 3 2p states, we only consider one of them, 2p_x in the following). Without the cavity, the energy difference between the 1s and the 2p states of the H atom is 0.375 and the energy difference is 1.5 in the case of the He⁺ ion. We want to study the behavior of the system when the cavity frequency is close to the 1s-2p energy difference. When using $L_x = 20, L_y = L_z = 406$ the lowest ω_k is 1.5 and $\lambda_k = 0.011$. In order to decrease the lowest ω_k to 0.375 we will set $L_x = 20, L_y = L_z = 1623$ which gives $\lambda_k = 0.0028$. As can be seen, decreasing the frequency makes λ_k significantly smaller (see Eq. (1)). The gap size, $L_x = 20$, is about 1 nm and the recently created subnanometer gap [2] picocavities make the $L_x = 10 - 20$ choice realistic. Below $L_x = 10$ the atomistic details of the cavity wall and the spill of the wave function of the H atom beyond the cavity wall would make the model unphysical.

The Fock space in Eq. (12) can quickly make the dimension of the Hamiltonian (in Eq. (13)) is unmanageable and truncation is needed. We will introduce a maximum frequency ω_{cut} and only $\omega_k < \omega_{cut}$ will be considered. Additionally, we have also tested that for coupling strengths up to $\lambda=0.1$, the occupation probability of the Fock states with $\sum_{k=1}^M n_k > 1$ are negligibly small ($< 10^{-8}$). Thus we will only use the photon-less $|0\rangle$ space and Fock spaces where only one $n_i = 1$ and the rest is zero. We will refer to the latter as ω_i space where all photon spaces are empty except for the ω_i space which has occupation number $n_i=1$.

To highlight the roles of different parts of the Hamiltonian we plot them in Fig. 1. The figure shows the magnitude of the different terms as a function of the cavity volume for an $L_x = L_y = L_z$ cavity. As Eq. (1) shows, the frequency is proportional to $V^{-1/3}$ and λ is proportional to $V^{-1/2}$. We will use $V^{-1/2}$ to show the volume dependence in the following. The ω_k frequencies change rapidly with decreasing the volume of the cavity (Fig. 1a). This term adds $n_k\omega_k$ energy to the total energy of the states containing photons but does not change the states besides the energy shift (see Eq. (14)). The coupling term (Eq. (16)) is proportional to $\sqrt{\omega}\lambda$ and contributes significantly to the Hamiltonian (Fig. 1b). One

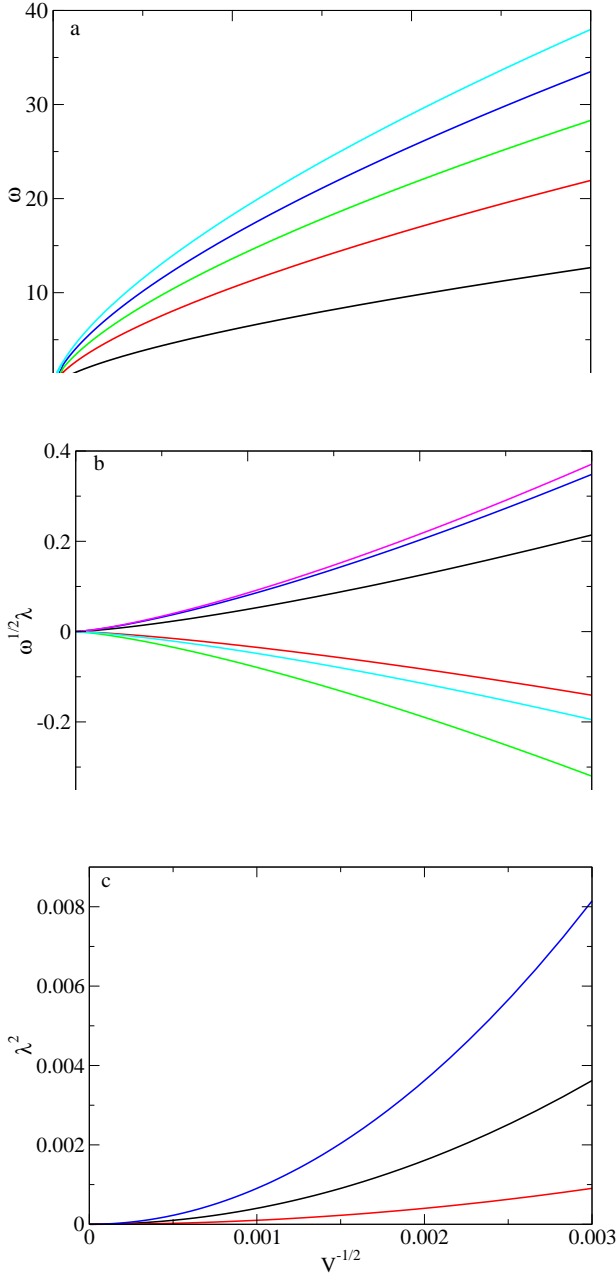


FIG. 1. a: Dependence of ω_k on $V^{-1/2}$. b: Dependence of $\sqrt{\omega_k}\lambda$ on $V^{-1/2}$. c: Dependence of λ^2 on $V^{-1/2}$. $L_x = L_y = L_z$ and the smallest volume is $L_x = 40$.

can see that the sign of the coupling term can be positive or negative leading to cancellations. The self-interaction term (the last term in Eq. (14)) is proportional to λ^2 (Fig.1c) and much smaller than the other terms.

A. Energy Spectrum

Fig. 2 shows the change of the energy of the H atom as the function of the volume of the cavity. The Fig. 2a figure zooms in the region where the cavity is large

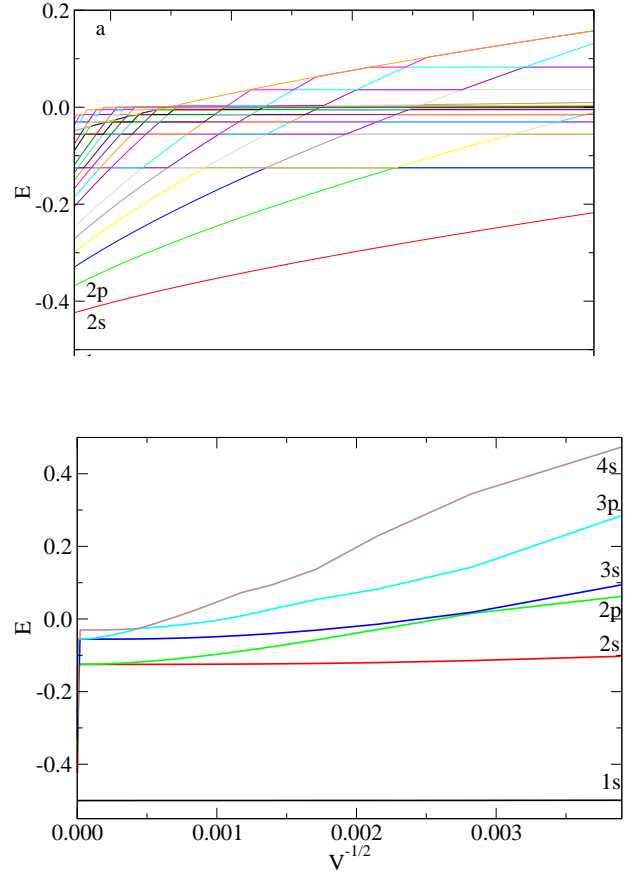


FIG. 2. a: Dependence of the energy on $V^{-1/2}$ in the $L=2000-8000$ region. b: Dependence of the energy on $V^{-1/2}$ in the $L=40-8000$ region.

and Fig.2b shows the full change when the cavity size is decreased to $L_x = L_y = L_z = 40$. In the larger cavity ($L_x = L_y = L_z = 2000, \dots, 8000$) the energy levels are raising quickly due to the strong effect of the $\omega_k n_k$ term in Eq. (14). The hydrogenic states (1s,2s,2p,...) are coupled to each ω_k state. The lowest line in Fig. 2 is the ground state coupled to the $|0\rangle$ photon-less state. The first excited state is the ground state of the Hydrogen atom coupled to the ω_1 ($|100, \dots\rangle$) state. The second excited state starts as a hydrogen ground state coupled to the ω_2 state but rises to reach the energy of the 2s state of the Hydrogen coupled to the $|0\rangle$ photon-less state. The coupling to any other photon states is negligibly small. When the energy of the two states get close to each other an avoided crossing occurs (this will be discussed later) and the second excited state becomes a 2s state coupled strongly to the photon-less state but with significant coupling to all other photon states. The entanglement with other photon spaces increases by increasing the coupling strength (decreasing the volume). Other higher excited states behave similarly, except that not only the photon spaces but the hydrogen eigenstates can also be coupled to each other with increasing the coupling strength.

Fig.2b shows the change of the lowest energy levels of

the Hydrogen when the cavity volume is decreased to $L_x = L_y = L_z = 40$. The state labels (1s,2s,2p...) are assigned based on the initial energy and angular momentum (when the coupling was very weak at the large volume limit). As the coupling increases these states become entangled states of hydrogenic and photonic states; each state is a linear combination of several coupled matter-photon states. The change of energy of the 1s state is small but it is coupled with all photon spaces. The 2s and 2p state start as degenerate states but the energy of the 2p state changes much more due to the dipole coupling. The figure also shows the avoided crossing between the 2p-3s and the 3p-4s states. The energy of higher excited states strongly depends on the light-matter coupling (cavity volume).

Fig.3 zooms in an avoided crossing region. Avoided crossing [52, 53] occurs when two energy levels approach each other but due to coupling between them the energy of the two states cannot be degenerated and will move on hyperbolic paths. The distance between the two paths is proportional to the coupling [54]. Fig.3 shows the change in the energy of the 1s and 2p states. Both of these states are coupled to the $|\mathbf{0}\rangle$ space and the ω_1 space which has one photon with frequency ω_1 and all other frequencies are unoccupied. We emphasize that all matter states and all photon states are coupled, and naming the matter states 1s or 2p means that the dominant component of the state is a 1s or a 2p state. The dominant components are strongly coupled to the $|\mathbf{0}\rangle$ space and the ω_1 photon states and the probability of other photon states are less than 0.001.

To show the avoided crossing we change the lowest cavity frequency ω_1 at around the 1s-2p excitation energy by fixing L_x and changing $L_y = L_z$ around 1623. Fig.3 shows that the energy of the lower 1s state nearly linearly increases up to 0.375 due to the ω_k term in Eq. (13) (see also Fig. 1a) and when it reaches its closest distance to the 2p states its slope decreases. The opposite is true for the 2p state, it starts flat and increases linearly after 0.375. The closest distance is not exactly at 0.375 because the energy difference between the two states is slightly different in the cavity. Fig. 3 shows the avoided crossing for two different cavity volumes. The gap increases by decreasing the cavity volume (increasing the coupling). As there are no states in the gap there is no light absorption for that energy (this is sometimes referred to as electromagnetically induced transparency). This gap is also called as Rabi splitting.

In this system, the avoided level crossing occurs not only between two states but between several states. Fig. 4 (same as Fig. 3 but now the 2s state is also included) shows the change of the energy levels with ω_1 . The figure shows that in addition to the avoided crossing between the 1s and 2p states, the 1s state also avoids the 2s state. The gap between the 1s and 2s state is very small because the coupling is small. The 1s and 2s state is not directly coupled (the dipole matrix element between these state is zero), but they are both coupled to other states, e.g.

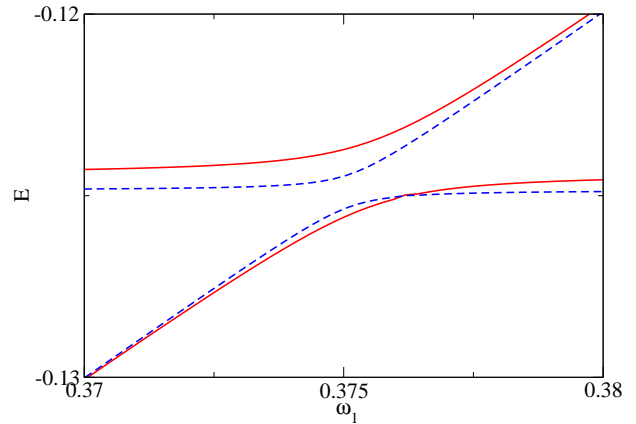


FIG. 3. Avoided level crossing as a function of ω_1 . The lowest frequency was tuned by changing $L_y = L_z$ around 1623 for $L_x = 20$ (solid line) and $L_x = 80$ (dashed line).

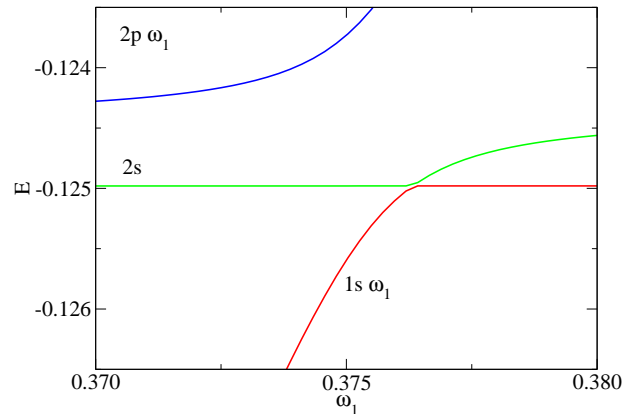


FIG. 4. Avoided level crossing as a function of ω_1 . The lines are labeled by the dominant matter state ($L_x = 20$).

the 2p state.

Fig. 5 shows how the photon occupation probabilities change at the avoided crossing. The 1s state (Fig.5a) is first coupled to the ω_1 state (that is why its energy increases linearly with ω_1 on Fig.4) and around the avoided crossing it is coupled to the ω_1 and $|\mathbf{0}\rangle$ states and after the avoided crossing it is fully coupled to $|\mathbf{0}\rangle$. The 2s state (Fig.5b) is coupled to the $|\mathbf{0}\rangle$ state and around the avoided crossing it coupled both to $|\mathbf{0}\rangle$ and ω_1 and returns to $|\mathbf{0}\rangle$ after that. The 2p state (Fig. 5c) is first coupled to $|\mathbf{0}\rangle$ only, it is coupled to both $|\mathbf{0}\rangle$ and ω_1 around the avoided crossing and finally it is only coupled to ω_1 . The 1s and 2p states switch coupling from $|\mathbf{0}\rangle$ to ω_1 between each other at the avoided crossing. The 2p state coupled to ω_1 continue to rise in energy and will reach a state above it leading to another avoided crossing and switching photon states.

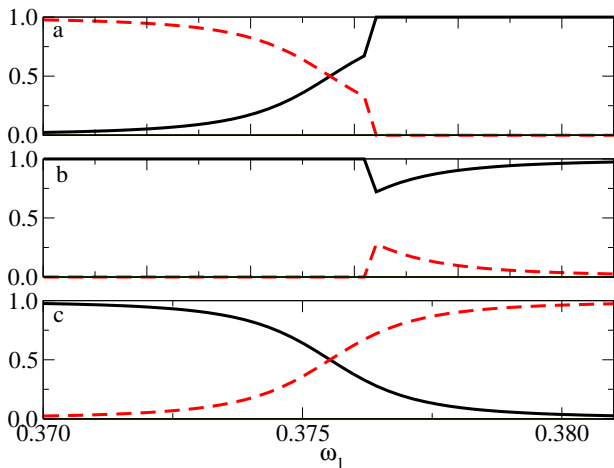


FIG. 5. Photon occupation probabilities in the $|0\rangle$ space (solid line) and in the ω_1 space which has one photon with frequency ω_1 and all other frequencies are unoccupied (dashed line) for the 1s (a), 2s (b) and 2p (c) states.

B. Optical absorption spectrum

In the cases we have discussed so far the energy spectrum was calculated by diagonalizing large sparse matrices with dimensions up to 10000. This is possible for a one-electron system, but not for larger atoms or molecules. In Ref. [19] we have introduced a QED time-dependent density functional theory (QED-TDDFT) calculations which solve a PF Hamiltonian using a product basis of a real space grid and a single Fock space. The present approach can be used to extend the QED-TDDFT to multiply photon spaces, but diagonalization is not possible in the QED-TDDFT case. To avoid diagonalization one can determine the excited states by calculating the optical absorption spectrum by solution of the time-dependent Schrödinger equation by time propagation. In the calculation, we start with a delta-kick perturbation (see eq. 28) which excites all states in the spectrum. In the following, we show examples of how the absorption spectrum changes in a cavity.

In Fig.6a we show the absorption spectrum peaks for a He^+ ion in a rectangular cavity for two different frequency cutoffs. The figure shows that the low energy peaks are not sensitive to the cutoff value and only the peaks close to the $E=2$ (continuum) threshold change somewhat. The cavity size is chosen so that the lowest cavity frequency is equal to the 1s to 2p transition energy ($\omega_1 = 1.5$). Using a lower frequency cutoff significantly reduces the basis dimensions and thus the calculation time.

Fig.6b shows the Rabi splitting of the 2p excited state of the He^+ ion in a cavity. The figure shows that when the volume of the cavity is large ($L_x = L_y = L_z = 406$) then there is only one peak at the 1s 2p transition in the absorption spectrum. By decreasing L_x to 20, λ_1 increases while the lowest cavity frequency remains the

same ($\omega_1 = 1.5$, because the frequency is determined by $L_x = L_y = 406$ choice). Due to the larger λ_1 the absorption peak splits into two peaks. By increasing λ_1 further ($L_x = 10$) gaps between the two peaks get larger. This is the same effect as the avoided crossing that we have shown in Fig. 3, but this time we show it using the absorption spectrum. The asymmetry of the peaks is due to the fact that the energy of the 1s 2p transition in the cavity is different from the (free space) analytical value and the difference increases with the coupling term.

Fig. 6c shows the same splitting for the 1s 3p transition of the He^+ ion. The cavity size is chosen so that the lowest cavity frequency corresponds to the 1s 3p transition energy ($E = 2 - 2/9$). The asymmetry of peaks is even larger in this case because the transition energy of the less tightly bound 3p state is more sensitive to the coupling to the cavity. The gap between the peaks is smaller than in the previous case and one would need stronger coupling to further increase the distance between the peaks.

Fig. 7 illustrates that any cavity mode can be used to split a peak in the absorption spectrum. In this case the second cavity mode, $\omega_2 = 1.5$ (generated by adjusting the size of the cavity) is used to split the 1s 2p transition peak. The figure also shows that longer time propagation leads the narrower peaks and after a very long time propagation Dirac-delta-like peaks would appear.

C. High Harmonic Generation

In atoms and small molecules, HHG can be understood as a three-step process [55, 56]. The laser removes the electrons from the system with tunnel ionization and when the direction of the driving field changes the electrons accelerate backward recombining and scattering with the parent ion. This process leads to a pulse train of attosecond radiation bursts. By Fourier transforming the temporal pulse train to the frequency space one gets a comb of harmonic peaks. These peaks appear at frequencies that are the integer multiples of the frequency of the exciting laser. These are not the only intensity peaks that we expect to observe in the HHG spectrum. Similarly to the absorption spectrum case, the strong laser also excites all states of the system, and peaks corresponding to the transitions between different energy levels will also appear in the HHG spectrum.

Fig.8 shows the HHG spectrum of the H atom in free space and in a cavity. The laser parameters are (see Eq. (26)) $E_0 = 0.01$, $\omega_h = 0.11395$, $t_0 = 15$ and $\tau = 8.8$. The figure shows the harmonic order which is defined as ω/ω_h (see Eq. (23)). In free space, due to the spherical symmetry, only the odd harmonics are allowed. Fig.8a shows the 1st, 3rd, ... 13th harmonics. The additional peaks are the excited states of the H atom, for example, the 1s 2p transition energy 0.375 appears at $0.375/\omega_h=3.3$, the 1s 3p transition is at $0.44444/\omega_h=3.9$. Fig.8b shows the HHG spectrum in a large cavity. The intensity of the peaks is much larger in this case and the peaks also

became wider due to the coupling with the cavity. Fig.8c shows the HHG spectrum when L_x is decreased to 20. The even harmonics are not forbidden anymore and they appear in the spectrum, while the odd harmonics are somewhat suppressed.

Fig.8 shows the total HHG calculated using all photon spaces, but using Eq. (25) one can calculate the HHG spectrum for the individual photon spaces as well. Fig.9 shows the HHG spectrum for the $|\mathbf{0}\rangle$, the ω_1 and the ω_2 photon spaces. The figure illustrates, that HHG spectrum is present in every photon spaces, although the intensity in the $|\mathbf{0}\rangle$ is larger.

Not only do atomic transitions appear in the HHG spectrum, but one can find states with energies corresponding to the cavity frequency as well. These states are coupled to matter states and appear in the spectrum in both the absorption and HHG cases. Fig.10 shows the peaks corresponding to the three lowest cavity modes for two different cavity sizes. The first (Fig.10a) is a larger cavity with lower frequency modes. The lowest three modes clearly show up with nearly equal intensity. Higher modes coincide with other peaks and are not visible. The second example (Fig.10b) shows the HHG for a smaller cavity with higher frequency modes. The calculations show that the appearance of peaks follows the change of cavity frequencies.

In the HHG calculations, we have shown the raw data without any smoothing. Various smoothing approaches are used in HHG calculations to hinder the noisy oscillations and reinforce the peaks. The HHG spectrum calculations are sensitive to the laser strength, duration, and pulse shape. Some of the oscillations can be removed by using a much longer laser pulse but that is computationally expensive. The peaks originating from the transition between coupled light-matter states appear with different intensities depending on the laser parameters.

In Figs.3 and 4 we have shown how an upper polariton (UP) and lower polariton (LP) is formed when the cavity frequency approaches a transition energy. Fig.11 shows how a laser field (Fig.11a) excites the LP and UP states. The calculation starts at $t = 0$ using the ground state wave function. In that state lowest 1s state coupled to the $|\mathbf{0}\rangle$ is the dominant configuration with 0.99 probability. This states remains the dominant configuration during the laser pulse. The laser excites other states but the probability of those states are much smaller. A stronger laser pulse could significantly decrease the population of the lowest state, but our goal here is the study of the LP and UP states. Fig.11b shows the $1s-\omega_1$ and the $2p-\omega_1$ during the laser pulse. Both states oscillate following the laser amplitude when ω_1 is below the $1s-2p$ transition energy, although the probability amplitude of the $1s-\omega_1$ state is much smaller. When ω_1 is close to the transition frequency, the $1s-\omega_1$ and the $2p-\omega_1$ state forms the LP and UP states. These are the same states that were studied in Fig.4. The laser excites both states similarly (Fig.11c) and the probability is nearly half of the non-resonant (Fig.11b, $\omega_1 = 0.3$) case. This last ex-

ample illustrates how the entangled light-matter states evolve during the laser excitation depending on the cavity modes. The dynamics of these coupled light-matter states build up the HHG spectrum of the system.

IV. SUMMARY

A coupled light-matter basis was used to calculate the properties of one electron systems in optical cavities. The electron's wave function was expanded in Gaussians which provides a flexible basis to describe excited states in laser fields. The light states are described by using a Fock representation. The PF Hamiltonian has a term, a product of the photon displacement operator and the matter dipole operator, that couples the light and matter. This term is conveniently handled by out tensor product basis of light and matter states.

We have shown how the light-matter states change as a function of the cavity size. The cavity dimension determines the cavity frequencies and the mode functions, ω_i and λ_i . In a small cavity λ_i is larger but ω_i also increases and it becomes much larger than the lowest transition states of the coupled system. This makes the manipulation of the resonances near transition energies more difficult. The coupled states are raising with increasing ω_i leading the a myriad of avoided level crossings (Rabi splittings). The example of 1s,2s, and 2p states shows that several energy level can repel each other at a single point due to the coupling to light.

The avoided level crossing appears as a Rabi splitting in the absorption spectrum. Due to the repulsion of the levels, there are no available states to absorb light in the energy gap leading to electromagnetically induced transparency. We have shown that any frequency mode in the cavity can be fine-tuned to split any absorption peak.

The effect of a cavity on the HHG spectrum was also studied. Strong coupling breaks the symmetry of the system and even harmonics can also appear. The energy spectrum of the light-matter coupled system is also imprinted in the HHG spectrum. This also means that there are HHG peaks at cavity frequencies which might be used to fine tune the emitted radiation. Besides the HHG peak at the integer multiples of the frequency of the exciting laser, one can create peaks at desired frequencies. The mark of the HHG spectrum can be found in all photon spaces, each photon carries information about the electronic levels of the emitter and the frequency of other photons as well.

The present approach was concentrated on a simple system where analytical matrix elements were available. This approach can also be used for the QED-TDDFT formed by tensor coupled real space and Fock space[19] extending the approach for multiple photon modes. Such calculations are under development in our group.

ACKNOWLEDGMENTS

This work has been supported by the National Science Foundation (NSF) under Grant No. 2217759.

-
- [1] I. Aupiais, R. Grasset, T. Guo, D. Daineka, J. Briatico, S. Houver, L. Perfetti, J.-P. Hugonin, J.-J. Greffet, and Y. Laplace, Ultrasmall and tunable terahertz surface plasmon cavities at the ultimate plasmonic limit, *Nature Communications* **14**, 7645 (2023).
- [2] J. J. Baumberg, Picocavities: a primer, *Nano Letters* **22**, 5859 (2022).
- [3] U. Bhattacharya, T. Lamprou, A. S. Maxwell, A. Ordóñez, E. Pisanty, J. Rivera-Dean, P. Stammer, M. F. Ciappina, M. Lewenstein, and P. Tzallas, Strong-laser-field physics, non-classical light states and quantum information science, *Reports on Progress in Physics* **86**, 094401 (2023).
- [4] A. Gorlach, M. E. Tzur, M. Birk, M. Kruger, N. Rivera, O. Cohen, and I. Kaminer, High-harmonic generation driven by quantum light, *Nature Physics* **19**, 1689 (2023).
- [5] A. V. Bogatskaya, E. A. Volkova, and A. M. Popov, Spontaneous emission of atoms in a strong laser field, *Journal of Experimental and Theoretical Physics* **125**, 587 (2007).
- [6] S. Wang and X. Lai, High-order above-threshold ionization of an atom in intense quantum light, *Phys. Rev. A* **108**, 063101 (2023).
- [7] J. Rivera-Dean, P. Stammer, A. S. Maxwell, T. Lamprou, E. Pisanty, P. Tzallas, M. Lewenstein, and M. F. Ciappina, Quantum-optical analysis of high-order harmonic generation in h_2^+ molecules, *Phys. Rev. A* **109**, 033706 (2024).
- [8] N. Moiseyev and M. E. Tzur, The conditions for the analog of qed photons in semi-classical periodically driven systems, *Journal of Optics* **26**, 025501 (2023).
- [9] A. V. Bogatskaya and A. M. Popov, Limitations of the semiclassical approach for the problem of two-level atomic ensemble emission in a resonant laser field, *Laser Physics Letters* **17**, 096002 (2020).
- [10] Z. Peng, H. Hu, J. Liu, J. Liu, Z. Zhao, and J. Yuan, Quantum radiation and absorption by current fluctuations of atoms in strong laser fields, *Phys. Rev. A* **108**, 053119 (2023).
- [11] T. W. Ebbesen, Hybrid light-matter states in a molecular and material science perspective, *Accounts of Chemical Research* **49**, 2403 (2016).
- [12] T. E. Li, B. Cui, J. E. Subotnik, and A. Nitzan, Molecular polaritonics: Chemical dynamics under strong light-matter coupling, *Annual Review of Physical Chemistry* **73**, 43 (2022).
- [13] M. Ruggenthaler, N. Tancogne-Dejean, J. Flick, H. Appel, and A. Rubio, From a quantum-electrodynamical light-matter description to novel spectroscopies, *Nature Reviews Chemistry* **2**, 0118 (2018).
- [14] J. McTague and J. J. Foley, Non-hermitian cavity quantum electrodynamics-configuration interaction singles approach for polaritonic structure with ab initio molecular hamiltonians, *The Journal of Chemical Physics* **156**, 154103 (2022).
- [15] M. Sánchez-Barquilla, A. I. Fernández-Domínguez, J. Feist, and F. J. García-Vidal, A theoretical perspective on molecular polaritonics, *ACS Photonics* **9**, 1830 (2022).
- [16] J. D. Mallory and A. E. DePrince, Reduced-density-matrix-based ab initio cavity quantum electrodynamics, *Phys. Rev. A* **106**, 053710 (2022).
- [17] A. Ahrens, C. Huang, M. Beutel, C. Covington, and K. Varga, Stochastic variational approach to small atoms and molecules coupled to quantum field modes in cavity qed, *Phys. Rev. Lett.* **127**, 273601 (2021).
- [18] C. Schäfer and G. Johansson, Shortcut to self-consistent light-matter interaction and realistic spectra from first principles, *Phys. Rev. Lett.* **128**, 156402 (2022).
- [19] J. Malave, A. Ahrens, D. Pitagora, C. Covington, and K. Varga, Real-space, real-time approach to quantum-electrodynamical time-dependent density functional theory, *The Journal of Chemical Physics* **157**, 194106 (2022).
- [20] C. Huang, C. Covington, and K. Varga, Harmonically confined n -electron systems coupled to light in a cavity: Time-dependent case, *Phys. Rev. B* **107**, 235130 (2023).
- [21] J. Malave, Y. S. Aklilu, M. Beutel, C. Huang, and K. Varga, Harmonically confined n -electron systems coupled to light in a cavity, *Phys. Rev. B* **105**, 115127 (2022).
- [22] C. Huang, A. Ahrens, M. Beutel, and K. Varga, Two electrons in harmonic confinement coupled to light in a cavity, *Phys. Rev. B* **104**, 165147 (2021).
- [23] A. V. Bogatskaya, E. A. Volkova, and A. M. Popov, Spontaneous emission from the atom stabilized by a strong high-frequency laser field, *Laser Physics* **27**, 095302 (2017).
- [24] A. Gombkötő, S. Varró, P. Mati, and P. Földi, High-order harmonic generation as induced by a quantized field: Phase-space picture, *Phys. Rev. A* **101**, 013418 (2020).
- [25] S. Varró, Quantum optical aspects of high-harmonic generation, *Photonics* **8**, 10.3390/photonics8070269 (2021).
- [26] A. Gombkötő, P. Földi, and S. Varró, Quantum-optical description of photon statistics and cross correlations in high-order harmonic generation, *Phys. Rev. A* **104**, 033703 (2021).
- [27] A. Gorlach, O. Neufeld, N. Rivera, O. Cohen, and I. Kaminer, The quantum-optical nature of high harmonic generation, *Nature Communications* **11**, 4598 (2020).
- [28] Y. Fang, F.-X. Sun, Q. He, and Y. Liu, Strong-field ionization of hydrogen atoms with quantum light, *Phys. Rev. Lett.* **130**, 253201 (2023).
- [29] J. Rivera-Dean, P. Stammer, A. S. Maxwell, T. Lamprou, P. Tzallas, M. Lewenstein, and M. F. Ciappina, Light-matter entanglement after above-threshold ionization processes in atoms, *Phys. Rev. A* **106**, 063705 (2022).
- [30] E. Jaynes and F. W. Cummings, Comparison of quantum and semiclassical radiation theories with application to

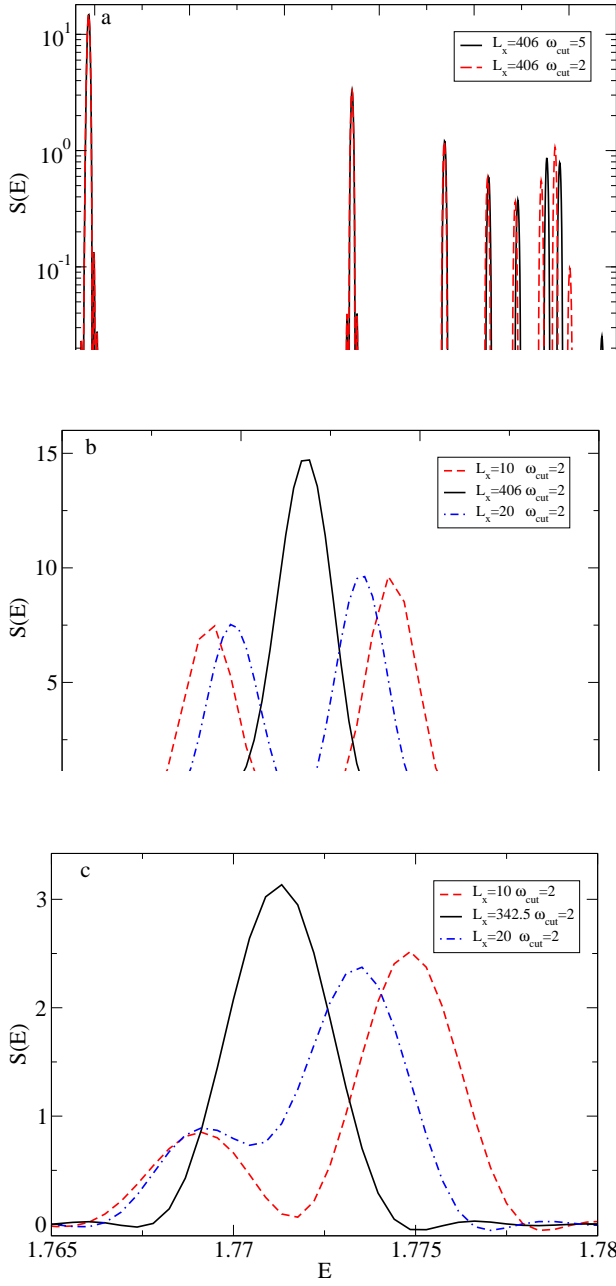


FIG. 6. a: Absorption spectrum for different values of ω_{cut} . The cavity size is $L_x = L_y = L_z = 406$ and $\omega_1 = 1.5, \omega_2 = 2.6, \omega_3 = 3.35, \omega_4 = 3.97, \omega_5 = 4.5, \omega_6 = 4.97, \lambda_1 = l, \lambda_2 = -l/2, \lambda_3 = -l, \lambda_4 = l, \lambda_5 = l, \lambda_6 = -l/2$ and $l = 0.0025$. b: Absorption spectrum showing the splitting of the $E = 1.5$ peak. The cavity size is $L_y = L_z = 406$ and L_x is varied. For $L_x = 20$ $\omega_1 = 1.5$ and $\lambda = 0.01$, for $L_x = 10$ $\omega_1 = 1.5$ and $\lambda = 0.015$. c: Absorption spectrum showing the splitting of the $E = 2 - 2/9 = 1.778$ peak. The cavity size is $L_y = L_z = 342.5$ and L_x is varied. $\omega_1 = 1.777$ for all L_x values. For $L_x = 342.5$, $\lambda_1 = 0.003$, $L_x = 20$, $\lambda_1 = 0.0131$, $L_x = 10$, $\lambda_1 = 0.0185$

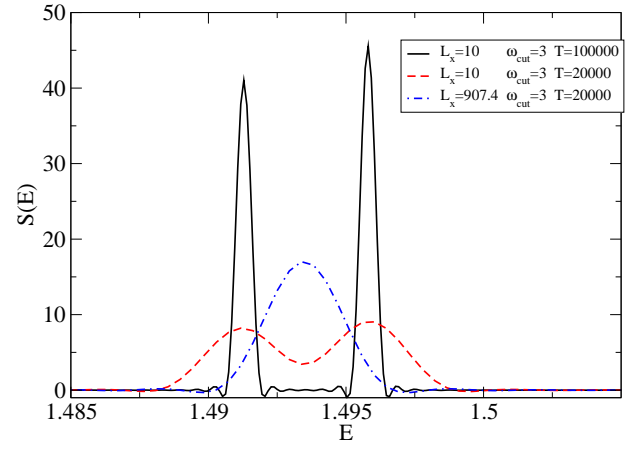


FIG. 7. Absorption spectrum showing the splitting of the $E = 1.5$ peak using the second photon mode. Cavity size $L_y = L_z = 907.4$ and L_x varied. $\omega_1 = 0.67, \omega_2 = 1.5, \omega_3 = 2.01, \omega_4 = 2.42, \omega_5 = 2.77, \lambda_1 = l, \lambda_2 = -l, \lambda_3 = l/2, \lambda_4 = l, \lambda_5 = -l, l = 0.007$

- the beam maser (1962).
- [31] F. Buchholz, I. Theophilou, S. E. B. Nielsen, M. Ruggenthaler, and A. Rubio, Reduced density-matrix approach to strong matter-photon interaction, *ACS Photonics* **6**, 2694 (2019).
- [32] C. Schäfer, M. Ruggenthaler, H. Appel, and A. Rubio, Modification of excitation and charge transfer in cavity quantum-electrodynamical chemistry, *Proceedings of the National Academy of Sciences* **116**, 4883 (2019).
- [33] J. Flick, M. Ruggenthaler, H. Appel, and A. Rubio, Kohn–sham approach to quantum electro-dynamical density-functional theory: Exact time-dependent effective potentials in real space, *Proceedings of the National Academy of Sciences* **112**, 15285 (2015).
- [34] J. Flick, M. Ruggenthaler, H. Appel, and A. Rubio, Atoms and molecules in cavities, from weak to strong coupling in quantum-electrodynamics (qed) chemistry, *Proceedings of the National Academy of Sciences* **114**, 3026 (2017).
- [35] V. Rokaj, D. M. Welakuh, M. Ruggenthaler, and A. Rubio, Light–matter interaction in the long-wavelength limit: no ground-state without dipole self-energy, *Journal of Physics B: Atomic, Molecular and Optical Physics* **51**, 03 (2018).
- [36] N. Rivera, J. Flick, and P. Narang, Variational theory of nonrelativistic quantum electrodynamics, *Phys. Rev. Lett.* **122**, 193603 (2019).
- [37] J. Flick and P. Narang, Cavity-correlated electron-nuclear dynamics from first principles, *Phys. Rev. Lett.* **121**, 113002 (2018).
- [38] N. M. Hoffmann, L. Lacombe, A. Rubio, and N. T. Maitra, Effect of many modes on self-polarization and photochemical suppression in cavities, *The Journal of Chemical Physics* **153**, 104103 (2020).
- [39] I. V. Tokatly, Conserving approximations in cavity quantum electrodynamics: Implications for density functional theory of electron-photon systems, *Phys. Rev. B* **98**, 235123 (2018).
- [40] J. Galego, F. J. Garcia-Vidal, and J. Feist, Many-molecule reaction triggered by a single photon in polaritonic chemistry, *Phys. Rev. Lett.* **119**, 136001 (2017).
- [41] A. Mandal, S. Montillo Vega, and P. Huo, Polar-

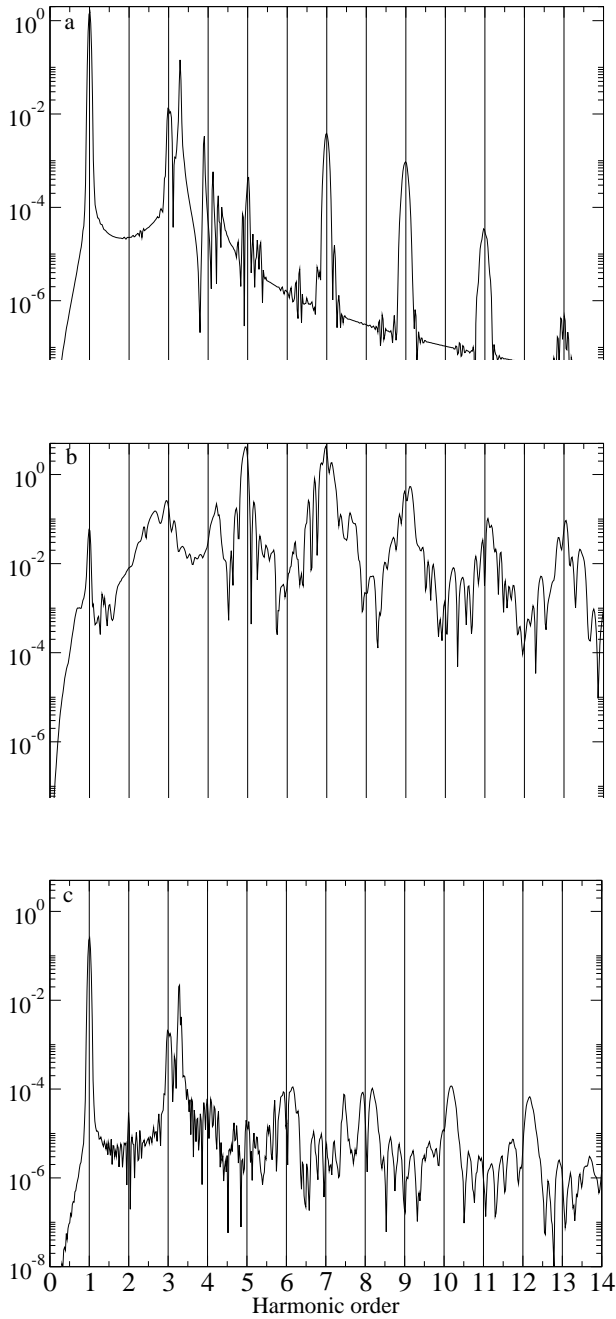


FIG. 8. (a) HHG spectrum for free (no cavity) H atom. (b) HHG spectrum for H atom in cavity $L_x = L_y = L_z = 4000$. (c) HHG spectrum for H atom in cavity $L_x = 20, L_y = L_z = 4000$. The vertical axis is I_h and the horizontal axis is $\omega\omega_h$.

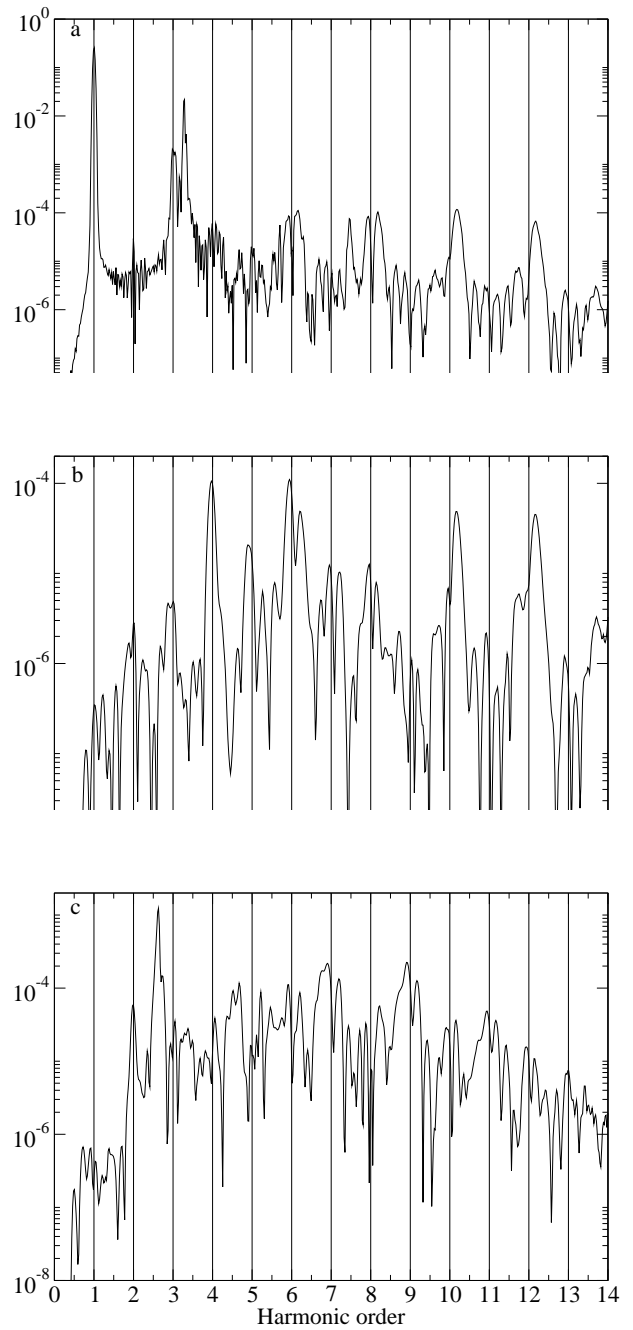


FIG. 9. HHG spectrum for the first (a) second (b) and third states (c) in a cavity of $L_x = 20, L_y = L_z = 2000$. The vertical axis is I_h and the horizontal axis is ω/ω_h .

ized fock states and the dynamical casimir effect in molecular cavity quantum electrodynamics, *The Journal of Physical Chemistry Letters* **11**, 9215 (2020), [44] pMID: 32991814.

[42] L. S. Cederbaum and A. I. Kuleff, Impact of cavity on interatomic coulombic decay, *Nature Communications* **12**, 4083 (2021).

[43] T. Szidarovszky, G. J. Halász, A. G. Császár, L. S. Cederbaum, and A. Vibók, Conical intersections

induced by quantum light: Field-dressed spectra from the weak to the ultrastrong coupling regimes, *The Journal of Physical Chemistry Letters* **9**, 6215 (2018).

[44] A. I. Ashida, Yuto and E. Demler, Cavity quantum electrodynamics at arbitrary light-matter coupling strengths, *Phys. Rev. Lett.* **126**, 153603 (2021).

[45] D. Craig and T. Thirunamachandran, *Molecular Quantum Electrodynamics; An Introduction to Radiation* (1984).

[46] A. Mandal, T. D. Krauss, and P. Huo,

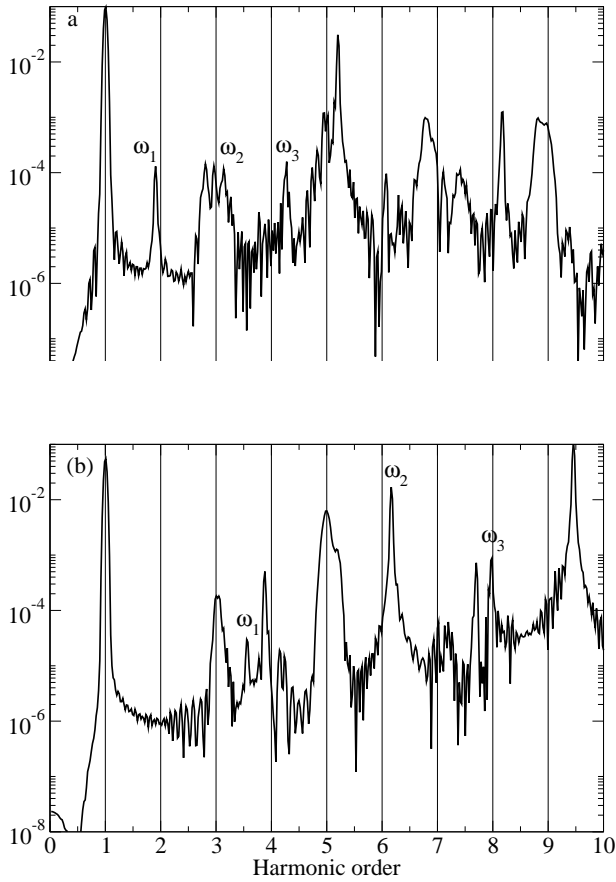


FIG. 10. (a) HHG spectrum in a cavity ($L_x = L_y = L_z = 2800$). The lowest cavity modes are $\omega_1/\omega_h = 1.91$, $\omega_2/\omega_h = 3.30$, $\omega_3/\omega_h = 4.26$. (b) HHG spectrum in a cavity ($L_x = L_y = L_z = 1500$). The lowest cavity modes are $\omega_1/\omega_h = 3.56$, $\omega_2/\omega_h = 6.16$, $\omega_3/\omega_h = 7.96$. The vertical axis is I_h and the horizontal axis is ω/ω_h .

Polariton-mediated electron transfer via cavity quantum electrodynamics, *The Journal of Physical Chemistry B* **124**, 6321 (2020), PMID: 32589846.

- [47] M. A. D. Taylor, A. Mandal, and P. Huo, Resolving ambiguities of the mode truncation in cavity quantum electrodynamics, *Opt. Lett.* **47**, 1446 (2022).
- [48] T. Pettersson and B. Hellsing, A detailed derivation of gaussian orbital-based matrix elements in electron structure calculations, *European Journal of Physics* **31**, 37 (2009).
- [49] S. F. Boys and A. C. Egerton, Electronic wave functions - i. a general method of calculation for the stationary states of any molecular system, *Proceedings of the Royal Society of London. Series A. Mathematical and Physical Sciences* **200**, 542 (1950).
- [50] J. Mitroy, S. Bubin, W. Horiuchi, Y. Suzuki, L. Adamowicz, W. Cencek, K. Szalewicz, J. Komasa, D. Blume, and K. Varga, Theory and application of explicitly correlated gaussians, *Rev. Mod. Phys.* **85**, 693 (2013).
- [51] Y. Suzuki, , and K. Varga, *Stochastic variational approach to quantum-mechanical few-body problems*, Vol. 54 (Springer Science & Business Media, 1998).
- [52] W. D. Heiss and A. L. Sannino, Avoided

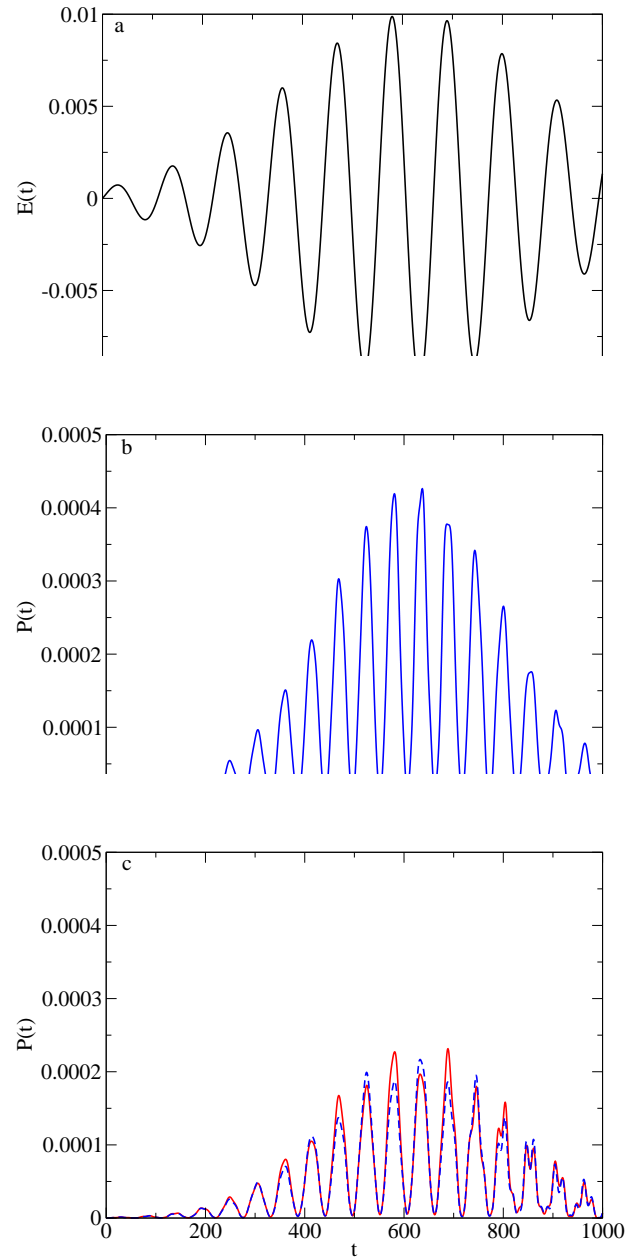


FIG. 11. (a) Laser field defined as $E(t) = E_0 e^{\frac{(t-T)^2}{\tau^2}} \sin(\omega_h t)$, with $E_0 = 0.01$, $\omega_h = 0.057$, $\tau = 8.8$, $T = 15$. (b) Evolution of the 2p state when the lowest frequency is 0.3. (c) Evolution of the LP (solid line) and UP (dashed line) when the lowest frequency is 0.375. The same cavity is used as for Fig. 3.

- level crossing and exceptional points, *International Journal of Physical Sciences* **200**, 542 (1950).
- [53] H. Eleuch and I. Rotter, Avoided level crossings in open quantum systems, *Fortschritte der Physik* **61**, 194 (2013).
- [54] I. Rotter, Dynamics of quantum systems, *Phys. Rev. E* **64**, 036213 (2001).
- [55] J. L. Krause, K. J. Schafer, and K. C. Kulander, Calculation of photoemission from atoms subject to intense laser fields, *Phys. Rev. A* **45**, 4998 (1992).

[56] M. Lewenstein, P. Balcou, M. Y. Ivanov, A. L'Huillier, and P. B. Corkum, Theory of high-

harmonic generation by low-frequency laser fields, Phys. Rev. A **49**, 2117 (1994).

